NONEQUILIBRIUM REACTIONS IN AN ARC IN A PERMEABLE CHANNEL WITH FAST GAS INJECTION

A. V. Pustogarov, D. I. Slovetskii, A. B. Karabut,
V. N. Sharshakov, and V. Yu. Vishnevskii

UDC 533.9

A study has been made on how parameters influence the target-product yields in plasmochemical reactions involving combining atmospheric nitrogen and converting carbon dioxide.

An arc in a permeable channel with vigorous gas injection can have parameters substantially different from equilibrium ones at atmospheric or elevated pressures [1, 2]; over much of the channel area, the electron temperature substantially exceeds the gas value, so the vibrational-excitation temperature is also higher than the latter. There are nonequilibrium electronically excited and charged-particle concentrations [2].

The factors causing deviations increase towards the periphery but they are not entirely clear; it has been suggested that turbulent pulsations in the gas flow and arc parameters play a major part, which in particular accelerate electron and vibrationally excited molecule transport. Interest attaches to how the disequilibrium affects reaction rates.

Here we report arc parameters for a permeable channel with vigorous injection of air or carbon dioxide and the effects on reactions giving oxides of nitrogen and carbon dioxide decomposition products.

Apparatus and Methods. Figure 1 shows the plasmotron and apparatus; the cathode 1 is a thermionic emission insert made of zirconium; part of the gas G_0 (1-5% of the total) is injected through the gap between the cathode body and cathode diaphragm 2 to stabilize the cathode spot. The main part of the gas G_p is injected through the porous wall in the electrode insert 3; the channel there is made of foam cordierite ($2MgO \cdot 2Al_2O_3 \cdot 5SiO_2$) [3]. The internal diameter d was varied over the range 10-28 mm. Diagnostic slots were present in the porous channel having heights exceeding the internal diameter, through which the radiation escaped. These slots were closed by the silica windows 4. The discharge was photographed by the high-speed camera 9. The additional shutter 7 was used because the uncontrolled exposure time provided by the electromagnetic shutter was 5-6 times the mirror rotation period.

The tungsten probes 6, diameter 0.5-0.8 mm, were inserted within the channel to a depth of 2-3 mm to determine the potential distribution; the signals passed along coaxial cables to a noninductive voltage divider 11 ($R = 2$ MΩ) and then to the electronic or loop oscilloscope 10. The gas pressure level in the channel was controlled by the throttle 16.

The gas was sampled for analysis in three different ways. In the first, a water-cooled copper sampler was used, which was placed at the anode 5. The sampling hole diameter was 2 mm, length 30 mm, and diameter 5 mm, taper angle 15°. The second involved quenching the entire gas flow emerging from the anode cavity by a copper water-cooled quencher 17 (149 channels, diameter 2.5 mm, length 76 mm). The calculated quenching rate was 10^7 K/sec with a gas flow of 1 kg/sec and a mean mass temperature 2500 K. The third was taking samples without quenching from the flow after the cooler 14. In all three cases, the samples were transmitted to a 0.8 liter stainless-steel vessel. This had first been evacuated to 10^3 Pa and was connected to the samplers. When the pressure had risen to 10^5-$2 \cdot 10^5$ Pa, the sampling was halted. The contents were analyzed with Tsvet-4 and Tsvet-6 chromatographs. A standard method was used to analyze the carbon dioxide decomposition products.

There were certain difficulties in measuring the nitrogen oxide concentrations, for which we used a column containing KSK-2.5 silica gel treated with 1.5 mass% oil, temperature 380 K [4]. The nitrogen dioxide is partially sorbed, but the peak has a tail, since NO_2, CO_2,

Translated from Inzhenerno-Fizicheskii Zhurnal, Vol. 54, No. 4, pp. 576-582, April, 1988. Original article submitted December 18, 1986.

0022-0841/88/5404-0394$12.50

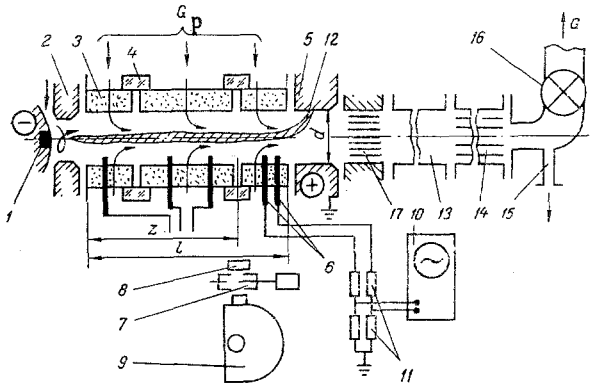

Fig. 1. The apparatus: 1) cathode; 2) cathode diaphragm; 3) porous channel; 4) window; 5) anode; 6) probe; 7) additional shutter; 8) interference filter; 9) VFU-1 high-speed camera; 10) S1-17 oscilloscope; 11) voltage divider; 12) discharge; 13) refractory tube; 14) cooler; 15) sampling; 16) throttle; 17) quenching device.

and N_2O emerge from the column at about the same time. We therefore used the [5] method to determine NO_2, in which the adsorbant was SKT charcoal, fraction 0.25-0.5 mm, impregnated with nickel sulfate (10 mass% in terms of the anhydrous salt). The effects of air on the N_2O and NO_2 analyses were excluded by using a glass column, part of which (about 0.1 m) was in an evaporator at 413-480 K. The evaporator temperature was varied to adjust the accuracy in determining NO_2. In that range, it was possible to prevent the dioxide dimerizing to N_2O_4, which causes measurement errors.

The sample was input with a syringe, which reduced the volume; the gas in the tank was diluted with helium to a pressure of $2\text{-}5\cdot10^5$ Pa to simplify chromatography. The samples were taken into the syringes through a rubber seal connected to a tube in the tank.

The chromatographs were calibrated and the analysis errors were determined by means of model mixtures; the relative error in concentration determination was 5-7%. The absolute sensitivity for nitrogen dioxide was better than 0.04 vol.%.

Discharge Characteristics. Gas-dynamic probes showed that the flow in the channel with porous-wall injection gave a flatter profile for the axial velocity by comparison with turbulent flow in a smooth tube with the same axial flow rate. The flattening increases with the specific injection and downstream (the axial flow stress increases) [6]. This flow pattern affects the interaction with the arc.

Figure 2 shows measurements on the potential U; the electric field E was determined by differentiating $U(\ell)$ graphically. In the anode section, which is less than a third of the total length, some 30-50% of the total potential difference is dissipated, and here E is maximal. As the specific input (flow rate) increases for air, the rate of increase in E along the channel rises and attains 250 V/cm. For a smooth channel with comparable parameters, E does not exceed 60 V/cm [7]. With carbon dioxide, there were similar U and E distributions.

High-speed photography (Fig. 3) showed that increasing the flow rate with the other parameters constant at first compressed the arc and reduced the visible diameter; then large-scale transverse oscillations occurred in the column as a whole (characteristic time 10^{-4} sec). At even higher flows, the column tended to break up into channels, with the central zone occupied by these channels tending to expand and the number of them increasing. These current channels arise, migrate, and die away (characteristic time 10^{-4}-10^{-6} sec) and produce relaxing small-scale plasma formations.

A nonequilibrium plasma is produced because of the high field strength and the transport of charged and excited particles followed by recombination on mixing with the cold gas [1, 2]. Calculations [8] show that charged-particle recombination in a medium having a low heavy-particle translational temperature (about $1\cdot10^3$ K) causes most of the energy to enter molecular vibrational levels. When the vibrational temperature exceeds the translational one, reactions may be substantially accelerated [9, 10]. A direct check was made on the nonequilibrium reaction-product yields for the oxides of nitrogen and the decomposition products from carbon dioxide.

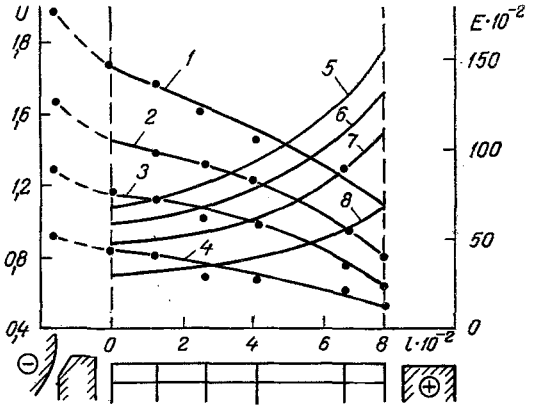

Fig. 2. Distributions of the potential U (1-4) and electric field E (5-8) along the channel in air (d = 20, ℓ = 80): 1, 5) G = 0.52, I = 525, p = 0.85; 2, 6) G = 0.34, I = 360, p = 0.45; 3, 7) G = 0.25, I = 305, p = 0.3; 4, 8) G = 0.14, I = 240, p = 0.12; d, ℓ, mm; G, kg/sec; I, A; p, MPa; U, kV; and E, V/cm.

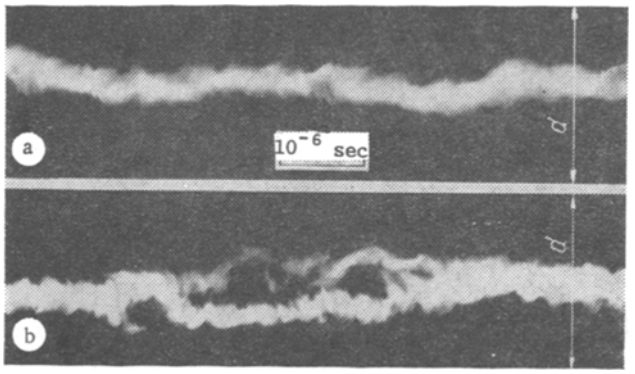

Fig. 3. High-speed photograph of arc in air (d = 20, ℓ = 80, section 45 mm from inlet): a) G = 0.12, I = 250, p = 0.27; b) G = 0.5, I = 450, p = 0.95.

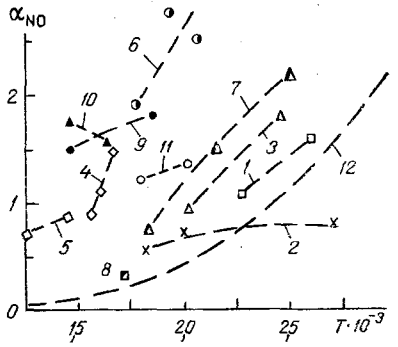

No. in fig.	d, mm	l, mm	G, kg/sec	I, A	p, MPa
1*)	28	150	0,1	300	0,2
2*)	28	94	0,25	360	0,4
3	28	150	0,33	450	0,86
4	28	150	0,52	440	0,85
5	28	150	0,77	400	1,05
6	28	94	0,25	325	0,4
7	28	94	0,34	460	0,55
8	20	80	0,12	230	0,25
9	20	80	0,34	360	0,6
10	20	80	0,25	300	0,4
11	20	80	0,52	450	0,95
12	Calc. for thermodynamic equilibrium [10].				

Fig. 4. Total yield of oxides of nitrogen (as NO) as a function of specific energy deposition under various conditions (α_{NO}, vol.%).*, without quenching.

Formation of Oxides of Nitrogen. The yields of these oxides are dependent on the sampling technique (Fig. 4); if there is no quenching on sampling, the yield is reduced by a factor 4-7 (curves 2 and 8 of Fig. 4). Quenching in the probe or in a quenching device gives the same result under similar conditions (curves 6, 9, and 10 in Fig. 4), so most of the experiments were performed with the quenching device. Complete mixing after quenching was provided, so the result represents the mean concentrations.

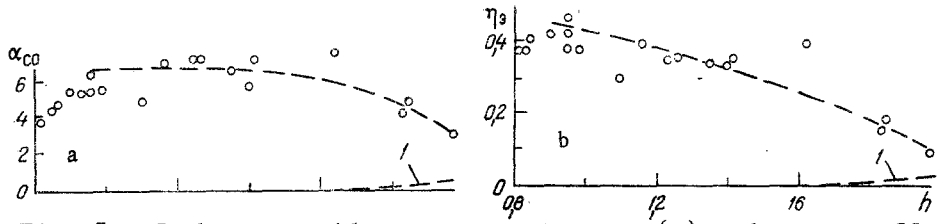

Fig. 5. Carbon monoxide concentration α_{CO} (a) and energy efficiency in carbon dioxide decomposition (b) as functions of specific energy deposition: 1) calculated for thermodynamic equilibrium [11], points from experiment, α_{CO} in vol.%, h in kJ/g.

A long channel with low injection gave near-equilibrium yields of the oxides (curve 1 in Fig. 4); as the injection increased, so did the disequilibrium (curves 3-5), which occurred also with shorter and narrower channels (curves 6-11). However, the dependence on the specific injection is nonmonotone. For constant energy deposition in a short channel, the yields at first increased with the specific injection (curves 8, 9, and 10) but then decreased (curve 11). A similar relationship occurred for a large-diameter channel (curves 6 and 7).

This indicates that the yields increase with the deviation from equilibrium, i.e., the greater the difference between the electron and gas temperatures, which increases with the field and specific injection and also as the diameter and length decrease at constant current. However, to obtain a constant specific energy deposition, one has to increase the current, which reduces the temperature difference because of rapid energy exchange between electrons and ions [2]. On these estimates, the zone having the highest energy deposition at 2 mm from the axis had a gas temperature for I = 300 A close to the mean mass value, whereas the electron temperature exceeded 10^4 K. Consequently, the vibrational temperature for the nitrogen substantially exceeded the gas value, and superequilibrium nitrogen-oxide concentrations occurred [9]. Quenching at rates over 10^7 K/sec with a probe or quenching device provided the nonequilibrium yields. In the absence of quenching, the yields falls to the equilibrium ones or even below them. Raising the current to 500 A can cause the gas and electron temperatures to equalize almost throughout the diameter, which reduces the nonequilibrium concentrations. Turbulent pulsations may increase the diffusion rates for the electrons, vibrationally excited molecules, and atoms, and can also do the same for the oxides of nitrogen formed in the peripheral cold zones, which should also increase the nonequilibrium yields. The efficiency in nonequilibrium nitrogen oxide synthesis under these conditions attains 6%, while the efficiency in the plasmotron was 91-95%.

Carbon Dioxide Dissociation. Figure 5 shows the results; quenching on sampling did not affect the dissociation. The energy efficiency η_e was calculated from the reaction enthalpy $\Delta H = 6.3 \cdot 10^3$ kJ/kg [9], while the CO contents were determined from the chromatography and from the power deposited. A check was made on the heat balance in the gas flow and in the input, which confirmed η_e within the error limits.

CO_2 decomposes to a large extent at low energy deposition, and the efficiency is high; the deviations from equilibrium, the degree of decomposition, and the efficiency increase as the deposition decreases. This shows that the dissociation is essentially disequilibrium.

In thermodynamic equilibrium at these deposition levels, the decomposition and the efficiency are very low, but they increase monotonically with the deposition; quenching had no effect on the carbon monoxide yield, which confirms the disequilibrium. Disequilibrium CO_2 dissociation in hf and uhf discharges produces higher degrees of decomposition and efficiencies ($\eta_e \approx 0.8$). The behavior of η_e as a function of deposition is determined by the plasma parameters, and it may be increasing or passed through a maximum in a given range [9].

These studies do not indicate all the mechanism details, but nevertheless, an arc with rapid gas injection through a permeable wall produces nonequilibrium CO_2 decomposition with high efficiency ($\eta_e = 0.4$) at pressures substantially higher than previously used in nonequilibrium hf and uhf discharges (0.15-0.4 MPa) and higher power levels (0.5 MW) [9].

NOTATION

U, voltage; I, arc current; E, electric field; G_0, cathode gas flow; G_p, gas flow through porous channel; G, total gas flow; d, internal channel diameter; ℓ, channel length; R, resistance; ΔH, reaction enthalpy; η_e, energy efficiency; p, pressure; α_{CO}, carbon monoxide concentration; α_{NO}, nitric oxide concentration.

LITERATURE CITED

1. Yu. V. Kurochkin, L. S. Polak, A. V. Pustogarov, et al., Teplofiz. Vys. Temp., No. 3, 485-491 (1978).
2. Yu. V. Kurochkin, L. S. Polak, A. V. Pustogarov, et al., Teplofiz. Vys. Temp., No. 6, 1167-1177 (1978).
3. Yu. V. Kurochkin, T. M. Lyubina, G. N. Mel'nikov, et al., Fiz. Khim. Obrab. Mater., No. 2, 128-133 (1981).
4. P. Jeffrey and P. Knipping, Chromatographic Gas Analysis [Russian translation], Moscow (1976).
5. T. Beskova and V. Filippov, Zavod. Lab., 38, 154-155 (1972).
6. M. F. Zhukov, A. S. An'shakov, M. I. Zasypkin, et al., Arc Generators Having Electrode Inserts [in Russian], Novosibirsk (1981).
7. A. B. Ambraziavičius, P. Yu. Valatkiavičius, A. I. Vilejšis, and R. A. Juškiavičius, Izv. Sib. Otd. Akad. Nauk SSSR, Ser. Tekh. Nauk, No. 8, Issue 2, 27-33 (1974).
8. L. M. Biberman, V. S. Vorob'ev, and I. T. Yakubov, Nonequilibrium Low-Temperature Plasma Kinetics [in Russian], Moscow (1982).
9. V. D. Rusanov and A. A. Fridman, Chemically Active Plasma Physics [in Russian], Moscow (1984).
10. A. S. Predvoditelev et al., Tables of Thermodynamic Functions for Air [in Russian], Moscow (1962).
11. D. I. Slovetskii, Reaction Mechanisms in Nonequilibrium Plasmas [in Russian], Moscow (1980).

INFLUENCE OF WEAKLY ABSORBING SOLID AEROSOL PARTICLES IN LOWERING THE OPTICAL BREAKDOWN THRESHOLD OF AIR

A. P. Prishivalko, L. G. Astaf'eva, and G. P. Ledneva

UDC 530.182.551.510.42

The influence of a subtance in the disperse state on the optical breakdown conditions of air is investigated.

The propagation of high-intensity laser radiation in the atmosphere is known to be accompanied by various kinds of nonlinear effects [1, 2], in particular, the optical breakdown of air. The presence of aerosol particles in the air usually lowers the threshold radiation intensity required for the initiation of optical breakdown by roughly two orders of magnitude. According to Zuev et al. [2, 3], the reduction of the optical breakdown threshold of air in the presence of absorbing disperse particles is caused by volatilization of the material of these particles when they are heated by laser radiation.

The present article is a theoretical investigation of the action of high-intensity laser radiation on weakly absorbing solid aerosol particles, whose presence can create conditions for lowering the optical breakdown threshold of air. The calculations are carried out for spherical particles of fused aluminum oxide with optical constants $m = 1.75 - i \cdot 10^{-7}$ and particle radii R = 7-17 μm. The wavelength of the incident radiation is $\lambda = 1.06$ μm. The energy density of the electric field both inside and outside the particle is characterized by the quantity B, which is expressed in terms of the electric field components

$$B = (\mathbf{E} \cdot \mathbf{E}^*)/|\mathbf{E}_0|^2. \quad (1)$$

Expressions for the components of the electric field in the interior of a spherical particle are given in [4, 5]. The components of the electric field for the diffracted near field can

Institute of Physics, Academy of Sciences of the Belorussian SSR, Minsk. Translated from Inzhenerno-Fizicheskii Zhurnal, Vol. 54, No. 4, pp. 582-585, April, 1988. Original article submitted October 16, 1986.

 0022-0841/88/5404-0398$12.50